Article

Synthesis of Diamond-Shape Titanate Molecular Sheets with Different Sizes and Realization of Quantum Confinement Effect during Dimensionality Reduction from Two to Zero

Eunju Lee Tae, Kee Eun Lee, Jong Seok Jeong, and Kyung Byung Yoon

J. Am. Chem. Soc., **2008**, 130 (20), 6534-6543 • DOI: 10.1021/ja711467g • Publication Date (Web): 18 April 2008

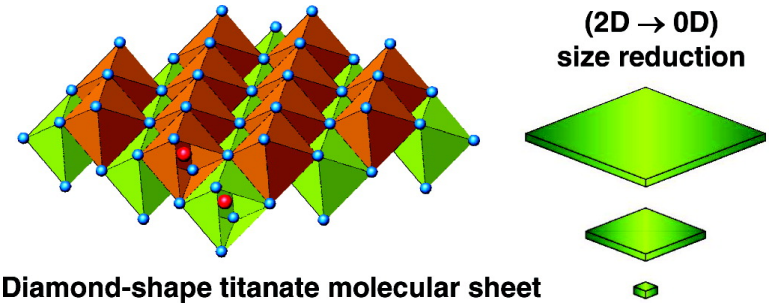

More About This Article

Additional resources and features associated with this article are available within the HTML version:

- Supporting Information
- Access to high resolution figures
- Links to articles and content related to this article
- Copyright permission to reproduce figures and/or text from this article

View the Full Text HTML

J|A|C|S
ARTICLES

Published on Web 04/18/2008

Synthesis of Diamond-Shape Titanate Molecular Sheets with Different Sizes and Realization of Quantum Confinement Effect during Dimensionality Reduction from Two to Zero

Eunju Lee Tae, Kee Eun Lee, Jong Seok Jeong, and Kyung Byung Yoon*

Center for Microcrystal Assembly, Department of Chemistry, and Program of Integrated Biotechnology, Sogang University, Seoul 121-742, Korea

Received January 6, 2008; E-mail: yoonkb@sogang.ac.kr

Abstract: Synthesis of semiconductor nanoparticles with uniform shapes, sizes, and compositions in series with a gradual size reduction has not been achieved for two-dimensional molecular sheets. We report a large-scale (>2.6 g) synthesis of 0.75-nm-thick diamond-shape lepidocrocite-type titanate molecular sheets with the sizes decreasing from (27.3, 19.1) to (7.7, 5.5), where the numbers in parentheses represent the long and short diagonal lengths, respectively, in nm. This is the first example of synthesizing semiconductor nanoparticles in series with the dimensionality reduction from two to zero, without coating the surfaces with surface-passivating ligands. The titanate molecular sheets showed three exciton-absorption bands in the 4.0–6.5 eV region, the absorption energies of which increased with decreasing the area. Contrary to the common belief, the per-unit cell oscillator strengths gradually increased with increasing area and the per-particle oscillator strengths increased in proportion to the area. The average reduced exciton masses along the two diagonal axes were 0.10 and 0.11 m_e, respectively, which were much smaller than those of bulk titanates (by 60–130 times). The estimated average Bohr radii along the two-diagonal axes were 4.8 and 4.3 nm, respectively.

Introduction

The current wide interest in nanoscience and nanotechnology[1] has evolved from the discovery of the quantum confinement effect (QCE) of nanometer-sized semiconductor materials:[2] the gradual increases in exciton absorption energy (E_{ex}) and oscillator strength (f) as the materials are gradually decreased to sizes comparable to or smaller than the Bohr radii of excitons (a_B) of the bulk semiconductor materials.[3–12] Therefore, to elucidate the important size−E_{ex} and size−f relationships and to extract the reduced mass of exciton (μ) and a_B from a semiconductor material, the semiconductor material should be synthesized in series with a gradual size reduction at the nanometer scale while keeping the composition, surface state, and shape of the particles the same. Interestingly, however, size reduction at the nanometer scale inevitably leads to changes in the material's dimensionality (D). Therefore, depending on D's of the starting and final materials, the direction of D change can be classified into six different types, as illustrated in Chart 1: (3D→2D), (3D→1D), (3D→0D), (2D→1D), (2D→0D), and (1D→0D), or more generally as (nD→lD), where n = 3, 2, or 1 and l = 2, 1, or 0 with $n > l$.

Ideally, nanometer-sized semiconductors have to be prepared in series in all six (nD→lD) directions with gradual size reductions to obtain the size−E_{ex} and size−f relationships, μ, and a_B for all (nD→lD) directions and to utilize them as important building blocks for various advanced materials. However, due to experimental difficulties, only 20 different types of semiconductors, namely, MoS_2,[13] WSe_2,[14] GaAs,[15,16] CdX (X = S, Se, and Te),[7a,9a,10–12,17–29] Si,[30] PbX (X = S, Se, and Te),[20,31–34] ZnX (X = O, S, and Se),[35–38] InX (X = P and As),[9b,39–43] CuX (X = Cl, Br, I),[8,18,19,44,45] Fe_2O_3,[46] and TiO_3^{2-} (titanate),[47] have successfully been prepared in series with

(1) (a) Schmid, G. *Nanoparticles: From Theory to Application*; Wiley-VCH: Weinheim; 2004. (b) Ozin, G. A.; Arsenault, A. C. *Nanochemistry: A Chemical Approach to Nanomaterials*; RSC Publishing: Cambridge, 2005.
(2) (a) Henglein, A. *Mechanism of Reactions on Colloidal Microelectrodes and Size Quantization Effects*; Hahn-Meitner-Institut Berlin Bereich Strahlenchemie: Berlin 1988. (b) Henglein, A *Chem. Rev.* **1989**, *89*, 1861–1873. (c) Yoffe, A. D. *Adv. Phys.* **1993**, *42*, 173–266.
(3) Brus, L. E. *J. Chem. Phys.* **1984**, *80*, 4403–4409.
(4) Takagahara, T. *Phys. Rev. B* **1987**, *36*, 9293–9296.
(5) Kayanuma, Y. *Phys. Rev. B* **1988**, *38*, 9797–9805.
(6) Hanamura, E. *Phys. Rev. B* **1988**, *37*, 1273–1279.
(7) (a) Wang, Y.; Suna, A.; McHugh, J.; Hilinski, E. F.; Lucas, P. A.; Johnson, R. D *J. Chem. Phys.* **1990**, *92*, 6927–6939. (b) Wang, Y.; Herron, N. *J. Phys. Chem.* **1991**, *95*, 525–532.
(8) Itoh, T.; Furumiya, M.; Ikehara, T.; Gourdon, C. *Solid State Commun.* **1990**, *73*, 271–274.
(9) (a) Rajh, T.; Mićić, O. I.; Nozik, A. J. *J. Phys. Chem.* **1993**, *97*, 11999–12003. (b) Yu, P.; Beard, M. C.; Ellingson, R. J.; Ferrere, S.; Curtis, C.; Drexler, J.; Luiszer, F.; Nozik, A. J. *J. Phys. Chem. B* **2005**, *109*, 7084–7087.
(10) Vossmeyer, T.; Katsikas, L.; Giersig, M.; Popovic, I. G.; Diesner, K.; Chemseddine, A.; Eychmüller, A.; Weller, H. *J. Phys. Chem.* **1994**, *98*, 7665–7673.
(11) Schmelz, O.; Mews, A.; Basché, T.; Herrmann, A.; Müllen, K. *Langmuir* **2001**, *17*, 2861–2865.
(12) Striolo, A.; Ward, J.; Prausnitz, J. M.; Parak, W. J.; Zanchet, D.; Gerion, D.; Milliron, D.; Alivisatos, A. P. *J. Phys. Chem. B* **2002**, *106*, 5500–5505.
(13) Evans, B. L.; Young, P. A. *Proc. R. Soc. Lond. Ser. A* **1967**, *298*, 74–96.
(14) Consadori, F.; Frindt, R. F. *Phys. Rev. B* **1970**, *2*, 4893–4896.
(15) Dingle, R.; Wiegmann, W.; Henry, C. H. *Phys. Rev. Lett.* **1974**, *33*, 827–830.
(16) Yu, H.; Buhro, W. E. *Adv. Mater.* **2003**, *15*, 416–418.

10.1021/ja711467g CCC: $40.75

Chart 1. Classification of Directions of Quantum Confinement and 20 Different Types of Semiconductors That Have Been Prepared in Series with Gradual Size Reduction along Each Direction

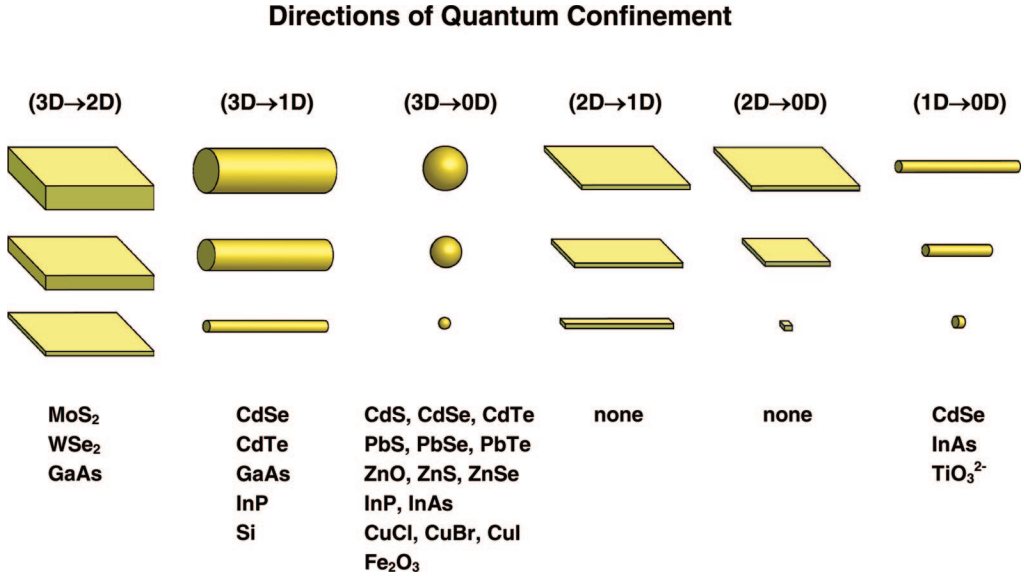

gradual size reductions along the (3D→2D),[13–15] (3D→1D),[16,27,29,30,41] (3D→0D),[7–12,17–24,26,28,31–39,42,44–46] and (1D→0D)[25,43,47] directions (Chart 1). In relation to the above, attempts have also been made in the preparation of semiconductor materials in series along the (3D→2D),[48] (3D→0D),[49] and (1D→0D)[50] directions.

Lepidocrocite[51]-type titanate[52] is an interesting layered titanate material that can be readily exfoliated into nanosheets. The lepidocrocite-type titanate sheets can even be produced on a platinum (110) surface by deposition of titanium and oxygen.[53] The chemical formula of the nanosheet is often represented as $M_xTi_{2-x/4}\Diamond_{x/4}O_4$, where M and ◊ represent a monovalent cation and the titanium vacancy, respectively, with $x \approx 0.7$.[52] Its lateral lattice parameters are 0.38 and 0.30 nm, respectively, with the thickness of ~0.7 nm.[52] The sizes of the resulting titanate

(17) Rossetti, R.; Ellison, J. L.; Gibson, J. M.; Brus, L. E. *J. Chem. Phys.* **1984**, *80*, 4464–4469.
(18) Ekimov, A. I.; Efros, A. L.; Onushchenko, A. A. *Solid State Commun.* **1985**, *56*, 921–924.
(19) Ekimov, A. I. *Phys. Scr.* **1991**, *T39*, 217–222.
(20) Wang, Y.; Herron, N.; Mahler, W.; Suna, A. *J. Opt. Soc. Am. B* **1989**, *6*, 808–813.
(21) Murray, C. B.; Norris, D. J.; Bawendi, M. G. *J. Am. Chem. Soc.* **1993**, *115*, 8706–8715.
(22) Yu, W. W.; Qu, L.; Guo, W.; Peng, X. *Chem. Mater.* **2003**, *15*, 2854–2860.
(23) Alivisatos, A. P.; Harris, A. L.; Levinos, N. J.; Steigerwald, M. L.; Brus, L. E. *J. Chem. Phys.* **1988**, *89*, 4001–4011.
(24) Klimov, V. I. *J. Phys. Chem. B* **2000**, *104*, 6112–6123.
(25) Li, L.-S.; Hu, J.; Yang, W.; Alivisatos, A. P. *Nano Lett.* **2001**, *1*, 349–351.
(26) Leatherdale, C. A.; Woo, W.-K.; Mikulec, F. V.; Bawendi, M. G. *J. Phys. Chem. B* **2002**, *106*, 7619–7622.
(27) Yu, H.; Li, J.; Loomis, R. A.; Gibbons, P. C.; Wang, L.-W.; Buhro, W. E. *J. Am. Chem. Soc.* **2003**, *125*, 16168–16169.
(28) Mastai, Y.; Hodes, G. *J. Phys. Chem. B* **1997**, *101*, 2685–2690.
(29) Tang, Z.; Kotov, N. A.; Giersig, M. *Science* **2002**, *297*, 237–240.
(30) Ma, D. D. D.; Lee, C. S.; Au, F. C. K.; Tong, S. Y.; Lee, S. T. *Science* **2003**, *299*, 1874–1877.
(31) Cademartiri, L.; Montanari, E.; Calestani, G.; Migliori, A.; Guagliardi, A.; Ozin, G. A. *J. Am. Chem. Soc.* **2006**, *128*, 10337–10346.
(32) Murray, C. B.; Sun, S.; Gaschler, W.; Doyle, H.; Betley, T. A.; Kagan, C. R. *IBM J. Res. Dev.* **2001**, *45*, 47–56.
(33) Lipovskii, A.; Kolobkova, E.; Petrikov, V.; Kang, I.; Olkhovets, A.; Krauss, T.; Thomas, M.; Silcox, J.; Wise, F.; Shen, Q.; Kycia, S. *Appl. Phys. Lett.* **1997**, *71*, 3406–3408.
(34) Urban, J. J.; Talapin, D. V.; Shevchenko, E. V.; Murray, C. B. *J. Am. Chem. Soc.* **2006**, *128*, 3248–3255.
(35) Haase, M.; Weller, H.; Henglein, A. *J. Phys. Chem.* **1988**, *92*, 482–487.
(36) Nanda, J.; Sapra, S.; Sarma, D. D. *Chem. Mater.* **2000**, *12*, 1018–1024.
(37) Smith, C. A.; Lee, H. W. H.; Leppert, V. J.; Risbud, S. H. *Appl. Phys. Lett.* **1999**, *75*, 1688–1690.
(38) Nikesh, V. V.; Lad, A. D.; Kimura, S.; Nozaki, S.; Mahamuni, S. *J. Appl. Phys.* **2006**, *100*, 113520.
(39) Guzelian, A. A.; Katari, J. E. B.; Kadavanich, A. V.; Banin, U.; Hamad, K.; Juban, E.; Alivisatos, A. P.; Wolters, R. H.; Arnold, C. C.; Heath, J. R. *J. Phys. Chem.* **1996**, *100*, 7212–7219.
(40) Mićić, O. I.; Ahrenkiel, S. P.; Nozik, A. J. *Appl. Phys. Lett.* **2001**, *78*, 4022–4024.
(41) Yu, H.; Li, J.; Loomis, R. A.; Wang, L.-W.; Buhro, W. E. *Nat. Mater.* **2003**, *2*, 517–520.
(42) Guzelian, A. A.; Banin, U.; Kadavanich, A. V.; Peng, X.; Alivisatos, A. P. *Appl. Phys. Lett.* **1996**, *69*, 1432–1434.
(43) Kan, S.; Mokari, T.; Rothenberg, E.; Banin, U. *Nat. Mater.* **2003**, *2*, 155–158.
(44) Ekimov, A. I.; Onushchenko, A. A. *Sov. Phys. Semicond.* **1982**, *16*, 775–778.
(45) Masumoto, Y.; Kawabata, K.; Kawazoe, T. *Phys. Rev. B* **1995**, *52*, 7834–7837.
(46) Park, J.; An, K.; Hwang, Y.; Park, J.-G.; Noh, H.-J.; Kim, J.-Y.; Park, J.-H.; Hwang, N.-M.; Hyeon, T. *Nat. Mater.* **2004**, *3*, 891–895.
(47) Jeong, N. C.; Lee, M. H.; Yoon, K. B. *Angew. Chem., Int. Ed.* **2007**, *46*, 1–6.
(48) Goto, T.; Maeda, J. *J. Phys. Soc. Jpn.* **1987**, *56*, 3710–3714.
(49) (a) Yamamoto, M.; Hayashi, R.; Tsunetomo, K.; Kohno, K.; Osaka, Y. *Jpn. J. Appl. Phys.* **1991**, *30*, 136–142. (b) Zhu, K.; Shi, J.; Zhang, L. *Solid State Commun.* **1998**, *107*, 79–84. (c) Fujii, A.; Ono, T.; Yu, W. *J. Phys. Soc. Jpn.* **2001**, *70*, 585–587. (d) Park, N.-M.; Choi, C.-J.; Seong, T.-Y.; Park, S.-J. *Phys. Rev. Lett.* **2001**, *86*, 1355–1357. (e) Jun, Y.-W.; Choi, C.-S.; Cheon, J. *Chem. Commun.* **2001**, 101–102. (f) Nakamura, Y.; Watanabe, K.; Fukuzawa, Y.; Ichikawa, M. *Appl. Phys. Lett.* **2005**, *87*, 133119. (g) Ding, L.; Chen, T. P.; Liu, Y.; Yang, M.; Wong, J. I.; Liu, Y. C.; Trigg, A. D.; Zhu, F. R.; Tan, M. C.; Fung, S. *J. Appl. Phys.* **2007**, *101*, 103525.
(50) Kanemitsu, Y.; Suzuki, K.; Nakayoshi, Y.; Masumoto, Y. *Phys. Rev. B* **1992**, *46*, 3916–3919.
(51) (a) Ewing, F. J. *J. Chem. Phys.* **1935**, *3*, 420–424. (b) Grey, I. E.; Li, C.; Madsen, I. C.; Watts, J. A. *J. Solid State Chem.* **1987**, *66*, 7–19.
(52) (a) Sakai, N.; Ebina, Y.; Takada, K.; Sasaki, T. *J. Am. Chem. Soc.* **2004**, *126*, 5851–5858. (b) Sasaki, T.; Ebina, Y.; Kitami, Y.; Watanabe, M.; Oikawa, T. *J. Phys. Chem. B* **2001**, *105*, 6116–6121. (c) Sasaki, T.; Watanabe, M. *J. Am. Chem. Soc.* **1998**, *120*, 4682–4689. (d) Sasaki, T. *Supramol. Sci.* **1998**, *5*, 367–371. (e) Sasaki, T.; Watanabe, M. *J. Phys. Chem. B* **1997**, *101*, 10159–10161.
(53) Orzali, T.; Casarin, M.; Granozzi, G.; Sambi, M.; Vittadini, A. *Phys. Rev. Lett.* **2006**, *97*, 156101.

nanosheets vary from a few hundred nanometers to several tens of micrometers. Despite their irregular sizes, they have received great attention as the components for lithium batteries,[54] building blocks for the fabrication of organic–inorganic composite materials through layer-by-layer assembly on substrates,[55] and intermediates to titanate nanotubes.[56] However, due to their irregularities in size and shape and due to their very large sizes, the interesting quantum confinement effects and the physical properties arising from the size (area) variation have not been elucidated.

We now report the synthesis of a series of nanometer-sized lepidocrocite-type titanate molecular sheets with a uniform thickness (0.75 nm) and shape (diamond), and with a gradual area reduction, which allowed us to demonstrate for the first time the complete size−E_{ex} and size−f relationships along the (2D→0D) direction. We also report the lateral μ and a_B values of the titanate molecular sheets and the relationship between size (area) and f.

Experimental Section

Materials and Procedure. Titanium tetraisopropoxide (TIP, Acros) and tetramethylammonium hydroxide (TMAOH, Sigma) were used as received. Syntheses of nanosheets were carried out by adding TIP (10 mL, 33.4 mmol) into an aqueous solution of TMAOH (273 mM, 150 mL) over a period of 5 min at room temperature. For samples A−J, the reaction mixture was stirred for 10 min and refluxed for varying periods: A, 0.5; B, 1; C, 3; D, 6; E, 9; F, 12; G, 15; H, 18; I, 21; and J, 24 h. Sample K was produced by addition of 5 mL of TIP into the hot solution of J and reflux for 24 h. Sample L was produced by addition of 10 mL of TIP into the hot solution of F and reflux for 24 h. Cesium lepidocrocite-type titanate was prepared by heating a mixture of Cs_2CO_3 (3.26 g, 10 mmol, Aldrich, 99%) and anatase (4.23 g, 53 mmol, Aldrich, 99.8%) at 1073 K for 20 h. After cooling to room temperature, the solid was finely ground using a mortar and pestle. The ground mixture was heated once again at 1073 K for 20 h. The reagents were used as received. Protonated lepidocrocite-type titanate was prepared according to the procedure of Sasaki's group[52c] after modification [see Supporting Information, SI-1 for its X-ray diffraction (XRD) pattern]. Thus, 250 mg of cesium lepidocrocite-type titanate was washed repeatedly with copious amounts of distilled deionized water until the pH of the supernatant solution was almost neutral. The washed cesium titanate (250 mg) was added into a plastic tube containing 10 mL of 1 M HCl. After shaking for 24 h, the solid particles were washed repeatedly with distilled deionized water until the pH of the wash was ∼5. The solid was collected by centrifugation and then dried at room temperature under vacuum. The XRD pattern matches well with that obtained by Sasaki's group.[52]

Transmission Electron Microscopy (TEM) Analyses. Each TMAOH solution of titanate molecular sheets was directly dripped onto a copper grid coated with a very thin carbon supporting film. Since the titanate molecular sheets were very thin, they easily underwent recrystallization upon admission of a strong electron beam during high-resolution (HR) TEM analyses. To minimize this, a small condenser aperture was used and the beam spot was adjusted to be as small as possible. The average lengths along the long (L_a) and short diagonal axes (L_b) of the nanosheets in each batch and their standard deviations (σ) were obtained by measuring the sizes of 50–70 nanosheets in the corresponding TEM images.

Atomic Force Microscopy (AFM) Analyses. Several pieces of Si wafer (10 × 10 mm^2) were cleaned by placing them in piranha solution for 1 h and subsequently washing with distilled deionized water. After drying in an oven at 100 °C for a few minutes, they were placed in a round-bottom flask charged with a dry toluene solution (50 mL) of 3-aminopropyl trimethoxysilane (0.1 mL) and subsequently refluxed for 10 min to covalently tether 3-aminopropyl groups on the Si wafer surfaces. The 3-aminopropyl-coated Si wafer plates were subsequently treated with methyl iodide to convert the 3-aminopropyl groups into trimethylpropyl ammonium groups with iodide as the counteranion $\{[(CH_3)_3N(CH_2)_3\text{-}]^+I^-\}$. The quaternary ammonium-coated Si wafer plates were dipped into a solution of titanate nanosheets (pH = 9) for 20 min, and the dipped plates were washed with distilled deionized water. The surfaces of the plates were subsequently analyzed with AFM.

Instrumentation. TEM and HRTEM images were obtained from a JEOL transmission electron microscope (JEM 4010) operated at 400 keV. AFM images of the monolayers of titanate nanosheets on Si wafer were obtained from a Veeco Nanoscope IV_a by tapping mode. The tip (RTESP) was operated at 250–300 KHz. X-ray powder diffraction patterns were obtained from a Rigaku D/MAX-2500/pc instrument. The X-ray diffraction pattern of the solution was taken from a Rigaku D/MAX-IIIC θ/θ goniometer. Raman spectra of the samples were recorded from a homemade setup equipped with an Ar^+ ion laser (Spectra-Physics Stabilite 2017) as an excitation beam source, a spectrometer (Horiba Jobin Yvon TRIAX 550), and a CCD detector (Horiba Jobin Yvon Symphony) cooled with liquid nitrogen. The wavelength of the excitation beam was 514.5 nm. The UV–vis spectra of the samples were recorded on a Varian Cary 5000 UV–vis−NIR spectrophotometer. Elemental analyses of Na and Ti were carried out with an elemental analyzer (Flash EA 1112 series, CE Instruments) located in the Korea Basic Science Institute.

Results and Discussion

Synthesis of Diamond-Shape Titanate Nanosheets with Uniform Sizes and Shapes. TEM images of the products (Figure 1, A−J) revealed the remarkable facts that, despite its simple procedure, the reaction readily produces diamond (lozenge)-shape nanosheets with internal angles of ∼77° and ∼103°, respectively (Chart 2), and that the nanosheets are highly uniform in size and shape. Accordingly, the nanosheets have a strong tendency to form closely packed arrays over larger areas on TEM grids (Figure 2). In the sense that TIP and TMAOH are used to produce titanium-containing oxide materials, our procedure is closely related to that of Chemseddine et al.[57] The significant difference between the two procedures is that, while we used 10 mL of TIP (33.4 mmol) and a highly concentrated aqueous TMAOH solution (273 mM, 150 mL), Chemseddine et al. used a much smaller amount (0.333 mL) of TIP and a much lower concentration of TMAOH (9.1 mM, 150 mL). As a result, while our procedure leads to the production of titanate nanosheets of uniform size and shape, their procedure leads to production of anatase nanoparticles of various sizes and shapes. These different results show that the reagent concentrations play crucial roles in determining the morphology and composition of titanium oxide species. It is also important to note that our procedure leads to the production of tangible amounts of products (>2.6 g), sufficient for immediate applications.

The long and short lateral axes of a diamond-shape nanosheet and the axis normal to the sheet are defined as a, b, and c axes,

(54) Bavykin, D. V.; Friedrich, J. M.; Walsh, F. C. *Adv. Mater.* **2006**, *18*, 2807–2824.
(55) (a) Sasaki, T.; Ebina, Y.; Tanaka, T.; Harada, M.; Watanabe, M. *Chem. Mater.* **2001**, *13*, 4661–4667. (b) Sasaki, T.; Ebina, Y.; Fukuda, K.; Tanaka, T.; Harada, M.; Watanabe, M. *Chem. Mater.* **2002**, *14*, 3524–3530. (c) Sasaki, T.; Ebina, Y.; Watanabe, M.; Decher, G. *Chem. Commun.* **2000**, 2163–2164.
(56) (a) Ma, R.; Bando, Y.; Sasaki, T. J. *Phys. Chem. B* **2004**, *108*, 2115–2119. (b) Ma, R.; Bando, Y.; Sasaki, T. *Chem. Phys. Lett.* **2003**, *380*, 577–582.
(57) Chemseddine, A.; Moritz, T. *Eur. J. Inorg. Chem.* **1999**, 235–245.

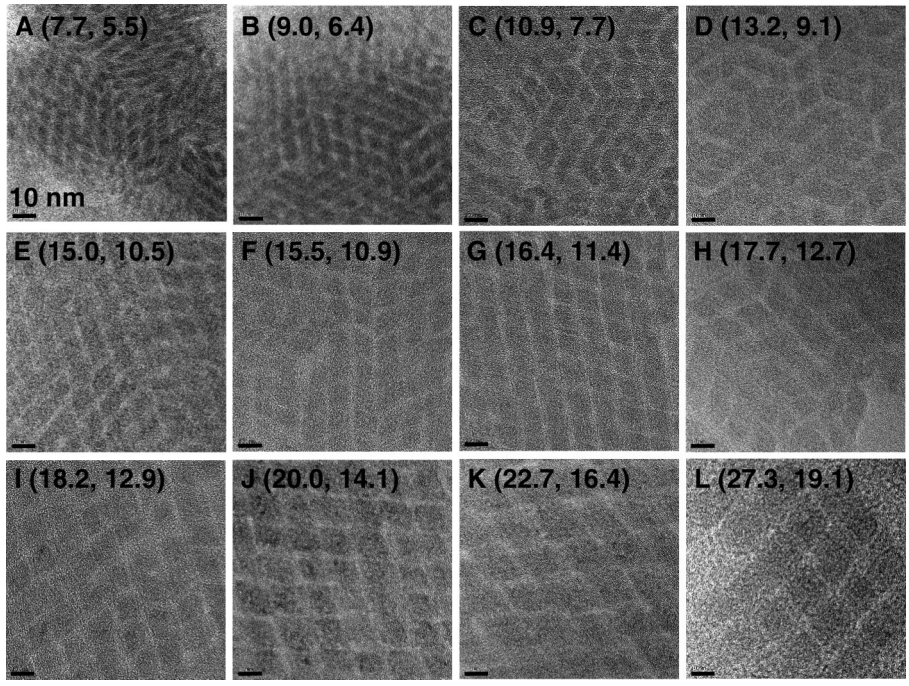

Figure 1. TEM images of closely packed arrays of diamond-shape nanosheets of uniform sizes, self-assembled on TEM grids. The diagonal lengths, L_a (long) and L_b (short), of each nanosheet are shown in parentheses.

Chart 2. Schematic Illustration of a Diamond-Shape Lepidocrocite and the Definitions of the Long and Short Diagonal Lengths and Thickness

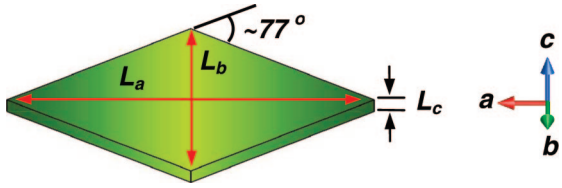

respectively (Chart 2). Accordingly, the lengths along the three axes are denoted as L_a, L_b, and L_c, respectively, in nanometers. On going from A to J, the lateral size (L_a, L_b) increased from (7.7, 5.5) to (20.0, 14.1), with the standard deviations less than 7.1% (Table 1). Interestingly, while the addition of 5 mL of TIP into the hot solution of J and continuation of the reflux for 24 h led to a further increase in size from (20.0, 14.1) to (22.7, 16.4) (Figure 1K), the addition of 10 mL of TIP (instead of 5 mL) into the hot solution of F (instead of J) led to a size increase to (27.3, 19.1) (Figure 1L). Thus, despite its simplicity, the above procedure readily produced titanate nanosheets of uniform (diamond) shape and size. Furthermore, the size was tunable either by increasing the reaction time or by adding additional amounts of TIP. Thus, the high concentration of TMAOH plays an important role in the formation of diamond-shape nanosheets.

TEM Analyses. The HRTEM images showed the existence of lattice planes in the nanosheets (Figure 3A). The magnified images revealed the presence of 0.19- and 0.15-nm interplanar spacings along the *a* and *b* axes, respectively (Figure 3B). The Fourier-transformed diffractogram of the magnified HRTEM image (Figure 3C) revealed the presence of three pairs of diffraction spots, which are indexed as 11, 20, and 02, respectively (*vide infra*). The ratio of the center-to-20 and center-to-02 distances was 15:19, which coincides with the inverse ratio of the interplanar spacings along the *a* (0.19 nm) and *b* (0.15 nm) axes. A TEM image of a group of nanosheets is shown in Figure 3D. The selected-area electron diffraction pattern showed a ring pattern (Figure 3D, inset), which is indexed as 11, 20, 02, and 22, respectively (*vide infra*). Some nanosheets were found as vertically oriented stacks of two or more (Figure 3E). Magnification (Figure 3F) revealed that the sheet thickness is ~0.75 nm (including two oxygen atoms with radius of ~0.14 nm) and the periodicity of the atomic arrangements along the *a* axis is 0.38 nm, which is the double of the spacing along the *a* axis (0.19 nm) in Figure 3B. The above TEM analyses revealed that the nanosheets are lepidocrocite-type titanate nanosheets and they exist on TEM grids as a single sheet or as stacks of a few sheets.

AFM Analyses. The AFM images of the titanate nanosheets [sample J, (20.0, 14.1)] supported on trimethylpropyl ammonium-coated Si plates revealed that the thicknesses of the nanosheets vary from 1.12 to 2.13 nm (SI-2, Supporting Information). Considering that TMA^+ ions (size ~0.4 nm) are likely to exist on top of the supported nanosheets for charge compensation, the images with thicknesses of ~1.12 nm are likely to represent single-layer nanosheets and those with thicknesses of ~2.13 nm are likely to represent double-layer nanosheets. The AFM results also show that the nanosheets tend to exist on solid supports (TEM grids and Si wafer) as a single sheet or as stacks of a few sheets.

X-ray Diffraction (XRD) Patterns. The lepidocrocite-type nanosheets readily precipitated as a white powder upon addition of ethanol (300 mL) into the solution. The XRD pattern of the precipitated powder showed the presence of two peaks at 48° and 62° (2θ), indicating the presence of interplanar spacings of 0.19 and 0.15 nm in the nanosheets (Figure 4A, bottom). The peaks at 48° and 62° still appear in the diffraction patterns of the nanosheets dispersed in aqueous TMAOH (273 mM) solutions of two different concentrations (with respect to Ti atom) (Figure 4A, middle, 670 mM; top, 220 mM). The lower angle peaks at $2\theta = 7.3$, 15.1, 25.9, 30.3, and 38.2° of the powder, those at $2\theta = 2.3$, 4.7, and 7.2° from the 670 mM solution, and those at $2\theta = 3.5$, 5.1, and 10.2° from the 220

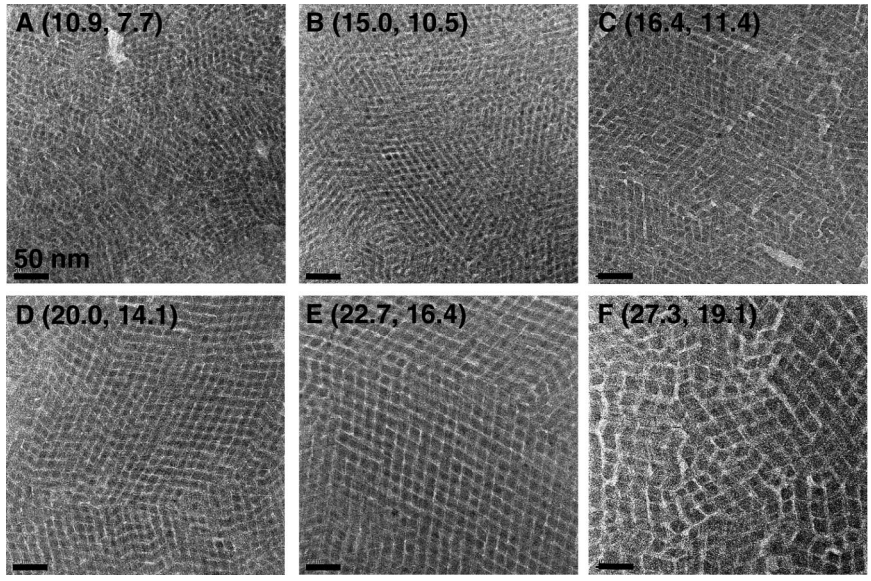

Figure 2. TEM images showing the arrays of larger numbers of titanate nanosheets assembled on TEM grids. The diagonal lengths, L_a (long) and L_b (short), of each nanosheet are shown in parentheses.

Table 1. Average Lateral Lengths (L_a and L_b), Standard Deviation (σ), Average Area, and Average Number of Unit Cells of the Nanosheets in Each Sample

molecular sheet	L_a (nm) (σ)	L_b (nm) (σ)	area (nm^2)	no. of unit cells
A	7.73 ± 0.27 (±3.5%)	5.45 ± 0.28 (±5.1%)	20.7	182
B	9.0 ± 0.49 (±5.4%)	6.36 ± 0.45 (±7.1%)	29.7	261
C	10.9 ± 0.40 (±3.7%)	7.73 ± 0.2 (±2.6%)	43.4	381
D	13.2 ± 0.89 (±6.7%)	9.09 ± 0.65 (±7.2%)	63.2	554
E	15.0 ± 0.45 (±3.0%)	10.5 ± 0.45 (±4.3%)	79.3	696
F	15.5 ± 0.91 (±5.9%)	10.9 ± 0.46 (±4.2%)	88.5	776
G	16.4 ± 0.40 (±2.4%)	11.4 ± 0.2 (±1.8%)	93.6	821
H	17.7 ± 1.2 (±6.8%)	12.7 ± 0.29 (±2.3%)	112	983
I	18.2 ± 0.91 (±5.0%)	12.9 ± 0.59 (±4.6%)	123	1078
J	20.0 ± 0.58 (±2.9%)	14.1 ± 0.55 (±3.9%)	143	1253
K	22.7 ± 0.91 (±4.0%)	16.4 ± 0.45 (±2.7%)	182	1596
L	27.3 ± 1.5 (±5.5%)	19.1 ± 1.1 (±5.8%)	268	2351

mM solution are assigned as the peaks that arise from the stacking of the nanosheets during precipitation and the transient stacking of the nanosheets in solution by equilibrium, respectively. The broad humps centered at $2\theta = 12°$, 27°, and 40° in the XRD patterns of both solutions arose due to TMA^+ ions, which are necessary to prevent the nanosheets from aggregation. Thus, consistent with the HRTEM results, the above XRD results confirmed the presence of the two lattice planes with the 0.19- and 0.15-nm interplanar spacings in the nanosheets. The results further revealed that the titanate nanosheets maintain their integrities both in the randomly stacked solid powders and in the dispersed state in TMAOH solutions. The result that the intensity of the XRD peak due to stacking is negligibly small at a nanosheet concentration of 220 mM indicates that most of the nanosheets exist individually as a single sheet in TMAOH solution at concentrations below 220 mM.

Raman Spectroscopy. The Raman spectrum of the precipitated powder ($\lambda_{exc} = 514.4$ nm) in the 150–1000 cm^{-1} region is shown in Figure 4B (bottom). For comparison, we independently prepared authentic H^+-exchanged lepidocrcite-type layered three-dimensional titanate, and its Raman spectrum in the above region is shown in Figure 4B (top).[58] The very close matching of the two Raman spectra further confirmed that the diamond-shape nanosheets are indeed lepidocrocite-type titanate sheets.

Theoretically, the diamond-shaped lepidocrocite-type titanate nanosheet with internal angles of 76.6° and 103.4° (Chart 2) is formed when the four edges of the nanosheet are finished with four energetically equivalent {11} planes. The perspective view and the simplified structure of a diamond-shaped lepidocrocite-type titanate nanosheet in various projections are shown in Figure 5A and B, respectively. The lateral unit cell dimensions are $a = 0.38$ nm and $b = 0.30$ nm, with an interaxial angle of ~90° (shaded area in Figure 5B, center), which includes two Ti atoms and four O atoms (Ti_2O_4). Consistently, the interplanar spacings along the a and b axes (0.19 and 0.15) in Figure 3B coincide with the halves of the corresponding unit cell dimensions.

The above results served as the basis for us to index the electron diffraction pattern of a single nanosheet in Figure 3C and the ring pattern in Figure 3D, inset. The absence of spot 22 in Figure 3C is ascribed to its very low intensity. The simulated HRTEM image of a lepidocrocite-type titanate nanosheet (along the c axis) coincides with the Fourier-filtered HRTEM image of a nanosheet (Figure 5C, inset: simulated image). The simulated HRTEM image of the simplified structure along the b axis ([01] projection in Figure 5B) also superimposes well with the HRTEM image of the nanosheet along the b axis

(58) Sasaki, T.; Nakano, S.; Yamauchi, S.; Watanabe, M. *Chem. Mater.* **1997**, *9*, 602–608.

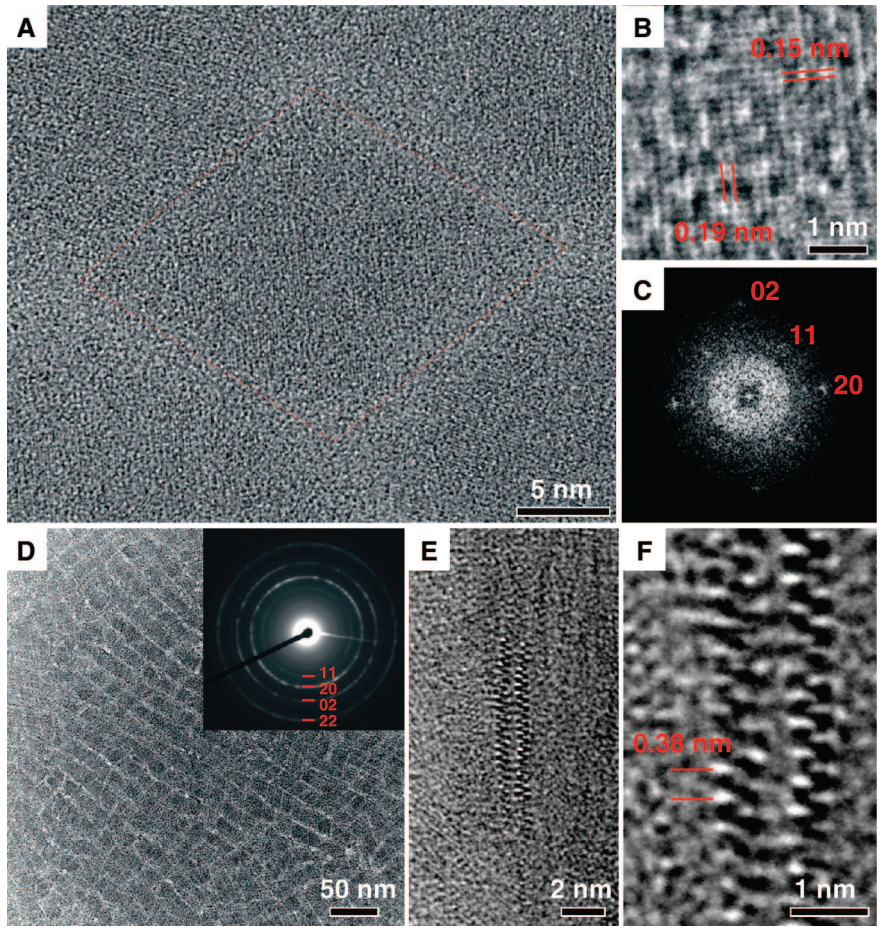

Figure 3. HRTEM image of a nanosheet viewed along the *c* axis (A), a magnified HRTEM image of a selected area of A (B), a Fourier-transformed diffractogram of B (C), a TEM image of the self-assembled nanosheets (D) (inset: selected-area electron diffraction pattern), a HRTEM image of a nanosheet viewed along the *a* axis (E), and a magnified image of E (F).

as compared in Figure 5D (inset: simulated). In relation to this, albeit very rarely, we also observed the side image along the *a* axis (Figure 5E; see SI-3, Supporting Information, for more detail). The above results further confirm that the structure of the diamond-shape titanate molecular sheets is indeed lepidocrocite-type.

Elemental Analysis. The chemical formula of a lepidocrocite-type titanate nanosheet is often represented as $M_xTi_{2-x/4}\Diamond_{x/4}O_4$, where M and ◊ represent a monovalent cation and the titanium vacancy, respectively, with $x \approx 0.7$.[52] In our case, the determined x values of sample D (13.2, 9.1) and sample H (17.7, 12.7) were 0.72 and 0.68, respectively. Therefore, the unit cell formula of our titanate nanosheets in TMAOH solution can be described as $TMA_xTi_{2-x/4}\Diamond_{x/4}O_4$, with $x \approx 0.7$.

Unpassivated Molecular Titanate Sheets. The above results of TEM, Raman, XRD, and elemental analysis unambiguously established that the nanosheets are indeed lepidocrocite-type titanate nanosheets with a uniform diamond shape and size, with the sizes varying from (7.7, 5.5) to (27.3, 19.1). The above lepidocrocite-type titanate nanosheets in TMAOH solution can also be described as titanate *molecular* sheets since their three dimensions, L_a, L_b, and L_c, are finite with lengths smaller than 30 nm and, in particular, since the number of atomic layers along the *c* axis is only four (Figure 5B). The titanate molecular sheets are good complements to the much wider lepidocrocite-type titanate sheets which have been prepared by exfoliation of the three-dimensional, protonated lepidocrocite-type titanate.[52] Furthermore, the exfoliated large titanate sheets are irregular in size, varying from a few hundred nanometers to several tens of micrometers.

Large-Scale Bottom-Up Procedure. Recently, lepidocrocite-type titanate sheets were produced on a platinum (110) surface by e-beam deposition of titanium and oxygen, and this procedure has been called a bottom-up procedure.[53] However, this procedure does not bear practical applicability. We believe that our method is a practically useful bottom-up procedure that also offers control of the size and shape of the sheets. The amount of product for each batch was higher than 2.6 g (excluding the organic cation), and, in fact, the yield can be readily increased by a mere scale-up. Thus, this large-scale synthetic method will expedite its immediate applications for catalysis and as building blocks for layer-by-layer assembly. We believe that the titanate molecular sheets with uniform sizes and shapes will exhibit more exciting and size-dependent physical properties during applications, which is a significant contribution to the science of titanate and titania. Our results also demonstrate that nanoparticles can be prepared in series with gradual size reduction from aqueous solutions at moderate temperatures in the absence of surface-passivating agents. We believe that a variety of other oxyanionic molecular sheets with different metal ions may also be produced by adopting our methodology.

Optical Properties. The (baseline-subtracted) UV–vis spectra of the diamond-shape titanate molecular sheets are shown in Figure 6A. For comparison, we also obtained the spectrum of

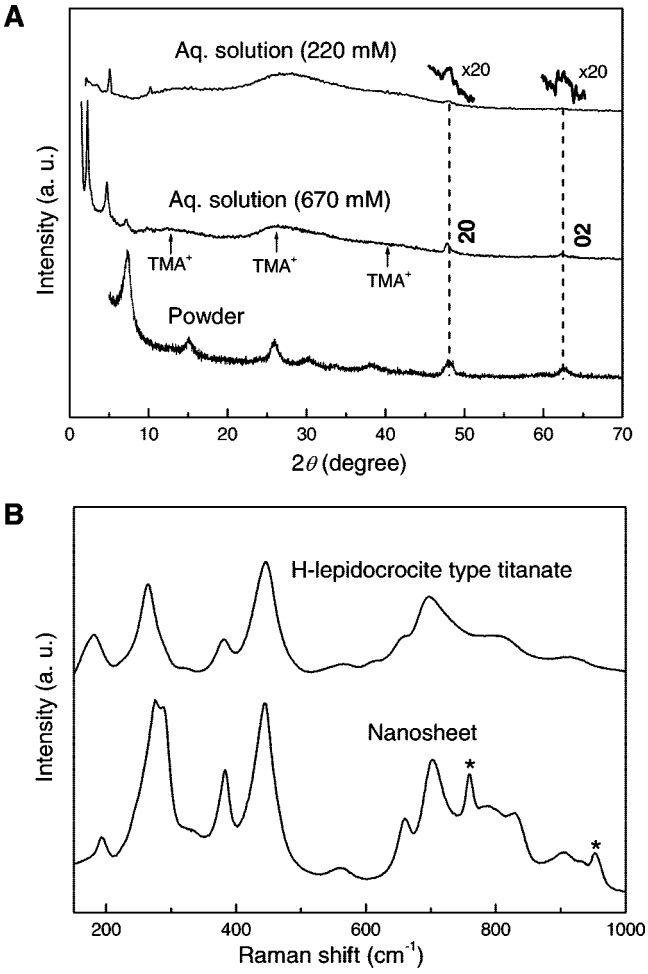

Figure 4. (A) XRD patterns of the powder obtained by precipitation of the nanosheet from the solution with ethanol (bottom) and aqueous TMAOH solutions of 670 mM (middle) and 220 mM (top). (B) Raman spectra of the solid obtained by precipitation of the nanosheet solution (bottom) and the protonated form of lepidocrocite-type titanate (top). The peaks with asterisks arise from TMAOH.

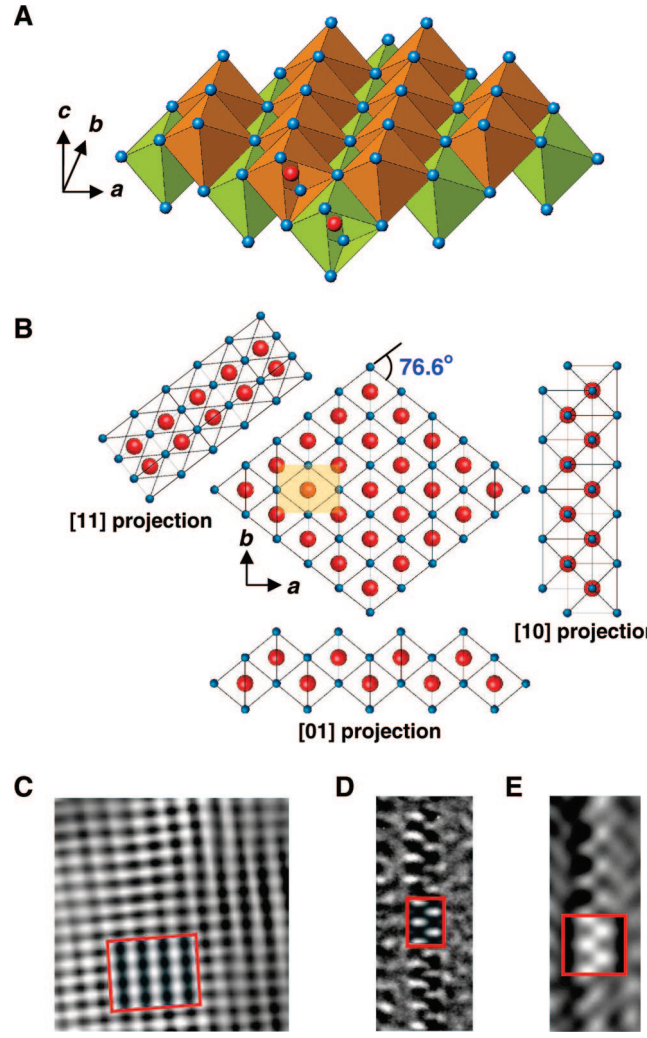

Figure 5. (A) Illustration of the perspective view of a lepidocrocite-type titanate molecular sheet. Blue balls, oxygen; red balls, titanium. (B) Projections of a lepidocrocite-type titanate molecular sheet along the [01], [10], and [11] directions and the view along the *c* direction (center). The shaded area in the center represents a unit cell. The theoretical internal angles are 76.6° and 103.4°, respectively. (C) Fourier-filtered image of a selected area of Figure 3B. Inset: Simulated HRTEM image of a lepidocrocite-type titanate molecular sheet viewed along the *c* axis (defocus, –290 nm; thickness, 0.5 nm). (D) A selected area of Figure 3F. Inset: Simulated HRTEM image of a lepidocrocite-type titanate molecular sheet viewed along the *b* axis (defocus, –240 nm; thickness, 11 nm). (E) HRTEM image of a lepidocrocite-type titanate molecular sheet viewed along the *a* axis. Inset: Simulated HRTEM image (defocus, –340 nm; thickness, 16 nm).

large titanate sheets dispersed in an aqueous tetrabutylammonium hydroxide solution according to Sasaki's procedure[52] and utilized it as the spectrum of bulk molecular sheets in the series. The spectrum of the bulk titanate sheets is overlaid onto those of the nanometer-size titanate molecular sheets. The absorption maximum and the spectral shape of the bulk molecular sheets coincide with those reported by Sasaki's group.[52] The concentrations (with respect to Ti atom) of all diamond-shape molecular sheets are fixed to 0.132 mM, regardless of the size. Only the concentration of the bulk titanate sheets is different (0.202 mM). The result clearly shows the interesting trend that the absorbance of titanate molecular sheets progressively increases as the area increases from (7.7, 5.5) to (27.3, 19.1).

Although the XRD pattern of the solution indicated that the diamond-shape molecular sheets exist in the TMAOH solution in the monomeric form up to a concentration of 220 mM (*vide supra*, Figure 4A), we measured the UV–vis spectrum of a titanate molecular sheet with a fixed size [sample K, (22.7, 16.4)] for the concentration range between 0.017 and 0.132 mM to confirm that the molecular sheets indeed exist in the monomeric form in solution (Figure 7). The reason the spectra look different from those in Figure 6A is that, while the spectra in Figure 6A are baseline-subtracted, those in Figure 7 are not. Indeed, the absorption maxima of the UV–vis spectra of the solutions remained constant in the above concentration range, indicating that the titanate molecular sheet remains monomeric in the solution (but not on a TEM grid or on a Si wafer) in the above concentration range. This result confirms that the spectra of the diamond-shape titanate molecular sheets are the spectra of monomeric titanate molecular sheets with different sizes (areas). It was noted that the extinction coefficient of the bulk titanate does not fit the trend of those of titanate molecular sheets. We ascribe this to the difference in their origins.

I. Exciton Band Shift. The UV–vis spectra indicated the presence of three exciton absorption peaks, which became more apparent after deconvolution (Figure 6B; see SI-4, Supporting Information, for more details). Their absorption maxima are

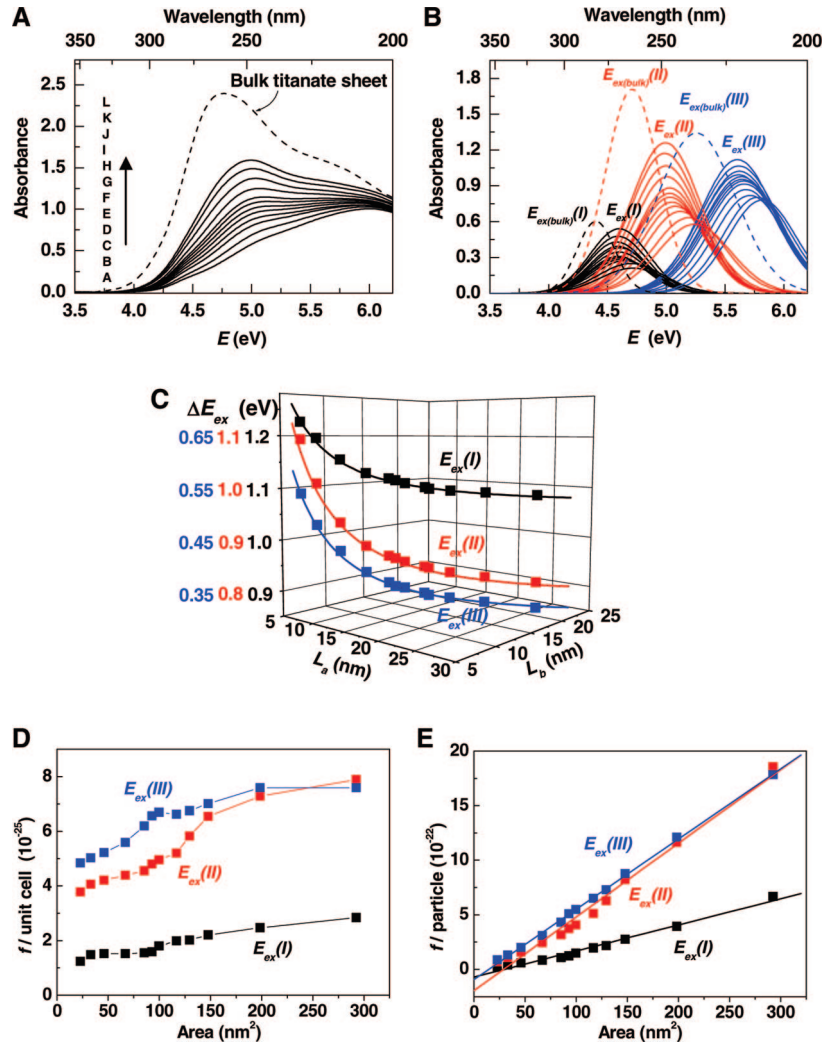

Figure 6. (A) Baseline-corrected UV–vis spectra of diamond-shape titanate molecular sheets with various sizes, as shown in Table 1. The dashed curve represents the spectrum of a bulk lepidocrocite-type titanate molecular sheet. (B) Three exciton absorption bands revealed by deconvolution of A. The dashed curves represent the deconvoluted spectra of bulk lepidocrocite-type titanate molecular sheets. (C) Relationship between ΔE_{ex} and L_a and L_b. (D) Relationship between per-unit-cell oscillator strength (*f*/unit cell) and area. (E) Relationship between per-particle oscillator strength (*f*/particle) and area.

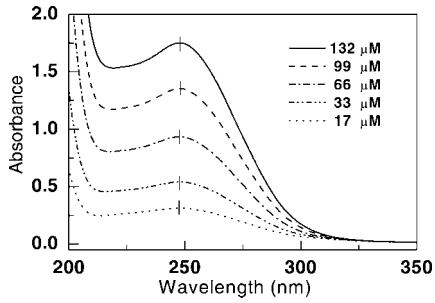

Figure 7. UV–vis spectra of the diamond-shaped titanate molecular sheets (baseline-uncorrected) with the average size of (22.7, 16.4) at different concentrations (as indicated).

denoted as $E_{ex}(n)$, where n = I, II, and III. The extracted $E_{ex}(n)$ are listed in Table 2. All three exciton absorption peaks gradually blue-shifted as the area of the molecular sheet decreased. From each E_{ex}value of the bulk, $E_{ex(bulk)}$ = I−III (4.4, 4.7, and 5.3 eV, respectively), $\Delta E_{ex}(n)$ [$E_{ex}(n) - E_{ex(bulk)}(n)$] were obtained for each n. The plots of $\Delta E_{ex}(n)$ with respect to L_a and L_b for a fixed L_c (0.75 nm) are shown in Figure 6C. The data sets were fitted with the effective mass approximation theory (eq 1),

$$\Delta E_{ex}(n) = E_{ex}(n) - E_{ex(bulk)}(n) = \frac{h^2}{8\mu_a L_a^2} + \frac{h^2}{8\mu_b L_b^2} + \frac{h^2}{8\mu_c L_c^2} \quad (1)$$

where h represents the Planck constant and μ_a, μ_b, and μ_c represent the effective reduced masses of excitons along the a, b, and c directions, respectively. Excellent matching between the fittings and the data sets was noted (Figure 6C).

In the cases of semiconductor nanoparticles coated with passivating ligands, the effective mass approximation theory has been shown to deviate from the experimental results, and the degree of deviation increases as the size of the nanoparticle decreases (in the strong confinement region).[7b,9a,20,21,28,33,36] On this basis, mass approximation theory has been criticized as being overly simplified. However, the excellent matching demonstrated in our case, despite the fact that the sizes of titanate sheets span between strong and medium confinement regions (*vide infra*), indicates the possibility that the effective mass approximation theory is in fact accurate enough to describe the size−E_{ex} relationships for unpassivated semiconductor nano-

Table 2. Exciton Absorption Energies (E_{ex}), Oscillator Strength (f), Per-Unit-Cell f, and Per-Particle f Extracted from the Three Exciton Bands Shown in Figure 6B

molecular sheet	$E_{ex}(n)$ (eV)			f (10^{-2})			f/unit cell (10^{-25})			f/particle (10^{-22})		
	I	II	III	I	II	III	I	II	III	I	II	III
A	1.226	1.083	0.542	3.85	11.8	15.0	1.24	3.78	4.84	0.23	0.69	0.88
B	1.196	1.001	0.482	4.59	12.6	15.6	1.48	4.06	5.02	0.39	1.06	1.31
C	1.156	0.927	0.432	4.72	13.1	16.2	1.52	4.21	5.22	0.58	1.60	1.99
D	1.131	0.882	0.392	4.72	13.6	17.4	1.52	4.39	5.59	0.84	2.43	3.10
E	1.121	0.863	0.372	4.81	14.2	19.2	1.55	4.55	6.19	1.08	3.17	4.31
F	1.117	0.858	0.364	4.94	14.9	20.4	1.59	4.80	6.56	1.23	3.73	5.09
G	1.112	0.851	0.362	5.59	15.4	20.8	1.80	4.96	6.69	1.48	4.07	5.49
H	1.104	0.841	0.350	6.19	16.2	20.6	1.99	5.20	6.62	1.96	5.11	6.51
I	1.101	0.839	0.347	6.27	18.1	21.0	2.02	5.82	6.75	2.17	6.28	7.28
J	1.098	0.831	0.342	6.86	20.4	21.8	2.21	6.54	7.01	2.76	8.20	8.78
K	1.094	0.821	0.332	7.68	22.7	23.6	2.47	7.28	7.59	3.94	11.6	12.1
L	1.090	0.812	0.322	8.83	24.6	23.6	2.84	7.89	7.59	6.68	18.6	17.8

particles. Conversely, the above excellent matching indicates that the deviations observed from surface-passivated nanoparticles are likely to arise from the perturbation of the nanoparticles by passivation, the degree of which is likely to increase as the particle size decreases. Indeed, it was demonstrated that the fitting of the experimentally observed size$-E_{ex}$ relationships with the mass approximation theory works better for unpassivated CuI nanoparticles embedded within a glass matrix.[45]

The μ values extracted from the three curves were $\mu_a = 0.11$, 0.04, and 0.15 m_e, $\mu_b = 0.14$, 0.12, and 0.07 m_e, and $\mu_c = 0.65$, 0.89, and 2.28 m_e. The average values of μ_a, μ_b, and μ_c were 0.1, 0.11, and 1.27 m_e, respectively. Interestingly, the obtained average μ_c was very similar to that obtained by Sasaki's group (1.28 m_e).[52] However, the determined lateral μ values of the titanate molecular sheet are smaller by ~60–130 times than those of three-dimensional titanates such as $MTiO_3$ (M = Ca, Sr, and Ba), which range between 6 and 13 m_e.[59] This reveals a remarkable phenomenon that the carrier mobility dramatically increases along the lateral directions as the material's dimensionality (D) changes from 3 to 2. It is also noteworthy that the average lateral μ values are ~10 times smaller than that of anatase ($\mu = 1$ m_e)[60] and 200–250 times smaller than that of rutile (μ = 20–25 m_e). However, when compared to the along-the-wire μ of one-dimensional titanate quantum wire embedded in porous silica (0.0006 m_e),[47] the observed lateral μ values are ~160 times larger. Thus, it can be concluded that the μ value of titanate decreases in the order of

$$3D > 2D > 1D$$

by a factor of 60–160 or ~2 orders of magnitude. The above results also clearly show the important phenomenon that the electron mobility increases as D decreases. From the results that the carrier mobility of the titanate molecular sheet is much higher than that of anatase (by ~10 times) and that two-dimensional molecular sheets offer higher surface areas than those of anatase, we predict that titanate molecular sheets are better materials for fabrication of dye-sensitized solar cells.[61]

The reported dielectric constant (ε) of bulk titanate nanosheets at λ= 300 nm is $9\varepsilon_o$, where ε_o is the vacuum permittivity.[52a] Assuming that ε is nearly constant in the spectral region between 310 and 200 nm, the estimated average a_B values along the a and b directions (a_{Ba} and a_{Bb}, respectively) from eq 2 are 4.8 and 4.3 nm, respectively.

$$a_B = \frac{\varepsilon h^2}{\mu \pi e^2} \tag{2}$$

The estimated lateral a_B values are much larger than the estimated a_B along the c direction (a_{Bc}, 0.37 nm)[52a] and those of anatase (1.5 nm)[62] and $CaTiO_3$ (2 nm),[59b] indicating that the size at which strong QCE appears is larger for 2D titanates than for the related 3D titania and titanates. Thus, this report provides novel insights into the physical properties of titania and titanate, which are important materials widely used in academia and industry. The estimated lateral a_B values further suggest that the diamond-shape lepidocrocite-type titanate molecular sheets span the strong and medium confinement regions, since $0.8 < L_a/2a_{Ba} < 2.9$ and $0.6 < L_b/2a_{Bb} < 2.3$.

II. Oscillator Strength Changes. The oscillator strengths $f(n)$, n = I, II, and III, for three exciton bands were also obtained from the titanate molecular sheets using eq 3,[10,63]

$$f = 4.32 \times 10^{-9} \int_{\nu_1}^{\nu_2} \varepsilon \, d\nu \tag{3}$$

where ε and ν represent the extinction coefficient (in cm^{-1} M^{-1}) and wavenumber (in cm^{-1}), respectively. They are listed in Table 2, along with per-unit-cell $f(n)$ and per-particle $f(n)$.[64] The concentration of the titanate molecular sheets for each size was measured with a very high accuracy from the corresponding absorption spectrum because the added Ti source (TIP, 0.132 mM) completely transformed into titanate molecular sheets under the reaction conditions, and the produced molecular sheets were highly monodisperse in shape and size. Interestingly, both per-unit-cell $f(n)$ and per-particle $f(n)$ gradually increased as the area of the molecular sheet increased (Figure 6D,E). In particular, per-particle $f(n)$ increased linearly in proportion to the area (or volume), with correlation factors of 0.9907, 0.9917, and 0.9992, respectively (Figure 6E), despite the fact that the sizes of the titanates belong to strong and medium confinement regions.

The relationships between per-unit-cell f and size and between per-particle f and size still remain controversial. Thus, in the case of spherical semiconductor quantum dots (in the case of

(59) (a) Berglund, C. N.; Baer, W. S. *Phys. Rev.* **1967**, *157*, 358–366. (b) Ueda, K.; Kawazoe, H.; Hosono, H. *Phys. Rev. B* **2000**, *61*, 7440–7447. (c) Linz, A.; Herrington, K. *J. Chem. Phys.* **1958**, *28*, 824–825.
(60) Tang, H.; Prasad, K.; Sanjinés, R.; Schmid, P. E.; Lévy, F. *J. Appl. Phys.* **1994**, *75*, 2042–2047.
(61) Hagfeldt, A.; Grätzel, M. *Acc. Chem. Res.* **2000**, *33*, 269–277.
(62) Wemple, S. H. *J. Chem. Phys.* **1977**, *67*, 2151–2168.
(63) Turro, N. J. *Modern Molecular Photochemistry*; Benjamin/Cummings: Menlo Park, CA; 1978; pp 86–87..
(64) Literally, the unit of $f$derived from eq 3 was cm^{-2} M^{-1}. However, it was treated as a unitless value in accordance with its definition.

3D→0D change), while the research groups of Brus,[3] Takgahara,[4] Kayanuma,[5] Hanamura,[6] Wang,[7] Itoh,[8] Nozik,[9] Yoffe,[2c] Weller,[10] Schmelz,[11] and Alivisatos[12] have theoretically proposed or experimentally demonstrated that per-unit-cell f is proportional to $1/r^3$ (r is radius) and per-particle f remains constant with respect to r in the strong and medium confinement regions, the research groups of Klimov,[24] Bawendi,[26] Peng,[22] and Ozin[31] showed that per-unit-cell f and per-particle f vary differently with varying sizes of quantum dots. In particular, Ozin and co-workers recently showed that per-particle f of PbS nanoparticles increases with respect to $r^{3.2}$, as if their sizes belong to the weak confinement region, despite the fact that their sizes are much smaller than a_B of PbS (16 nm).[20] Therefore, it can be said that titanate molecular sheets and PbS behave similarly in the sense that their per-particle f values increase in proportion to volume (or area).

Overall, this report describes the synthesis of a series of 0.75-nm-thick diamond-shape lepidocrocite-type titanate molecular sheets with the lateral diagonal lengths varying from (7.3, 5.5) to (27.3, 19.1), in nanometers. The yield for each batch is higher than 2.6 g, which can be considered to be large-scale. The titanate molecular sheets show three exciton absorption bands, $E_{ex}(n)$, $n = \mathrm{I}-\mathrm{III}$. Each E_{ex} increases with decreasing area. The plot of ΔE_{ex} with respect to the lateral dimensions L_a and L_b can be analyzed with the effective mass approximation theory. The estimated average μ_a, μ_b, and μ_c values were 0.10, 0.11, and 1.27 m_e, respectively. The estimated average a_{Ba} and a_{Bb} were 4.8 and 4.3 nm, respectively. Per-unit-cell oscillator strength increased with increasing area, and per-particle oscillator strength increased linearly with respect to the area (or volume). This is the first example to demonstrate QCE along the 2D→0D direction and to show the ability to synthesize nanoparticles in series with a gradual size reduction from the aqueous solution without coating the surface with surface-passivating agents. We believe that the novel lepidocrocite-type titanate molecular sheets with uniform shape and size will serve as useful components for fabrication of composite materials.

Acknowledgment. We thank the Ministry of Science and Technology (MOST) and Sogang University for supporting this work through the Acceleration Research and the Internal Research Fund programs, respectively. We thank Dr. Myoung Hee Lee for helpful discussions. We also thank Ms. Jiyun Lee for preparing the illustrations.

Supporting Information Available: X-ray diffraction pattern of H-lepidocrocite and simulated and experimentally observed HRTEM images of the side views of the lepidocrocite-type titanate molecular sheet. This material is available free of charge via the Internet at http://pubs.acs.org.

JA711467G